Computers Math. Applic. Vol. 20, No. 4–6, pp. 199–206, 1990
Printed in Great Britain.

0097-4943/90 $3.00 + 0.00

A MATHEMATICAL MODEL OF THE CIRCLE OF WILLIS IN THE PRESENCE OF AN ARTERIOVENOUS ANOMALY

C. J. PAPAPANAYOTOU,[1] Y. CHERRUAULT[1] and B. DE LA ROCHEFOUCAULD[2]
[1]MEDIMAT, Université P. et M. Curie, 15 rue de l'Ecole de Médecine, 75270 Paris Cedex 06, France
[2]Hôpital de la Pitié, Service de Biophysique, 83 blvd de l'Hôpital, 75013 Paris, France

Abstract—This paper deals with a complete model of the flow in the Willis circle and its vicinity. We study: (a) the normal case; and (b) the influence of the presence of an arteriovenous anomaly. We have simulated the therapeutic procedures in order to confirm the treatment.

1. INTRODUCTION

The haemodynamics of the circle of Willis have been studied by many authors. Physical models as well as mathematical ones have been designed to study the behaviour of this vascular circle.

In 1947, Rogers [1] experimented with a steady-flow model, later, in 1961, Avman and Bering [2] designed a mechanical model using pulsatile flow, followed by Streeter *et al.* [3] who presented the basic equations for elastic tube wall material and for continuity and momentum, including fluid frictional resistance of the wall of the tubes, based on one-dimensional flow. These equations were used to simulate pulsatile pressure and flow through distensible vessels. Murray [4] employed an electrical analogon with steady-flow conditions, as did Fasano *et al.* [5], the latter also used a hydraulic analogon.

The group of Clark and Himwich [6–11] started modelling the circle, with steady flow and rigid tubes, and arrived at numerically solved mathematical models of unsteady flow in flexible vessels. Most of these models were designed for the dog circle, as were the analog and digital computer models of Chao and Hwang [12, 13]. Duros and Nadvornik [14] investigated, using a computer model, the influence of the different parameters on the haemodynamics of the circle.

Hillen *et al.* [15] presented a mathematical model designed to study the haemodynamics of one posterior communicating artery and its afferent and efferent vessels. They later [16] extended their model to the study of the flow in the circle of Willis.

Kufahl and Clark [17] developed a numerical mathematical model of the arterial network surrounding the circle of Willis and of the circle itself.

Following the work of Collins and co-workers [18, 19], Zagzoule and Marc-Vergnes [20] presented a complete model of the cerebral circulation. In these studies all the segments of the circle of Willis were included. The purpose of the studies was to study the behaviour of the system in pathological situations. The lack of unanimity of these authors leads to the general conclusion that, because of its morphological variations, no predictions can be made concerning the functioning of the circle after occlusion of one of the afferent vessels [16].

Clark *et al.* [8] formulated four criteria for the design of models of the cerebral circulation:

1. An adequate description of the geometry of the circle of Willis.
2. Some estimate of the total flow through the circle.
3. An adequate representation of the pressure gradients for the afferent circle and efferent portions of the model.
4. An estimate of the division of the flow in the afferent vessels.

The first criterion is imperative and includes most of the last three criteria. Pressure gradients and the division of the flow are determined in part by the geometry and in part by the peripheral resistances, as is the total flow.

Our approach to the problem is to simplify the system to such a degree that we can study its basic principles in relation to the variation of morphology, mainly in the presence of an AVM. Our aim is to build a model that could become a surgeon's tool by which one could examine the

benefits of various types of surgery or compare the results of the same surgery performed in different ways.

For the purposes of estimating the time-dependent pressure and flow distribution due to steady or pulsatile flow, it is sufficient to formulate a quasilinear one-dimensional model in which flow profiles (velocity and pressure) are averaged over local cross-sections of the arterial segments.

2. THE CIRCLE OF WILLIS AND THE AVM

In health, the circle of Willis (Fig. 1), considered as the main distribution centre of the cerebral flow, distributes blood proportionately to the various sectors of the brain, this proportioning is first accomplished by the way in which the fluid resistances are distributed in the normal vasculature and in the capillary beds. In the case of disease, the circle acts as a safety device to maintain brain function, even though the total supply of blood is decreased or increased by an obstruction, haemorrhage or the presence of an AVM.

Vascular shunts that have been present (AVM) since birth create a compensatory equilibrium which can be upset by any therapeutic procedure. Knowing the local size, arterial feeders and draining veins of an AVM is not sufficient to decide the most appropriate treatment: one must also be conversant with the haemodynamic factors stabilizing the long-established relationship between the brain and the AVM in order to predict, and therefore prevent, the complications which may arise from any type of radical treatment.

To determine the consequences of an AVM on the cerebral blood volume and its autoregulatory capacity, the haemodynamics [systolic rate (VS) and diastolic rate (VD)] of the internal carotid artery blood flow can be determined by pulsed Dopper combined with ultrasound scans to measure the instantaneous blood flow in patients. Ancri and Pertuiset [21] showed that measurement of the diastolic fraction, $DF = (VD)^2/VS$, appears to be a valid method for assessing the severity of this malformation and the importance of its outputs. The values of the systolic and diastolic rates multiplied by the section of the corresponding vessel give the instantaneous systolic and diastolic volume fluxes.

Pertuiset *et al.* [22] used the pulsed Doppler technique for measuring the flow velocity in the cervical portions of the common and internal carotid arteries (ICAs). They found an increased volume flux in the arteries that fed an AVM and noted the volume flux variation post-operatively.

A comparative study on patients [23] developed before and after radical open surgery showed a significant reduction of DF after removal of the AVM. Comparisons between pre- and post-operative values strongly suggest that measuring the blood flow velocity in the ICAs provides a very close estimate of flow rate in the malformation.

In a group of patients whose angiograms showed that the AVM was fed by both ICAs through the anterior communicating artery, an Aesculap clip was placed on that vessel. The values of DF before and after clipping showed that the blood flow is not reduced by the closure of an important feeder. The increase in flow velocity observed, was probably due to the ICA on the same side as the AVM delivering blood for both arteries. In such cases the risk of haemorrhage during and after surgery is controlled by means of a special clamp reducing the flow in the ICA feeding the AVM; thus, the surgery is facilitated because only one carotid system has to be controlled instead of two.

Nies [24] and Hassler [25] presented their studies on the AVM's haemodynamics. Nies [24] notes that the flow velocity increases in the common carotid on the same side as the AVM. Diastolic rates are significantly increased and diastolic rates are also increased but to a lesser degree. Their values decreased significantly after radical surgery.

Hassler [25] experimented on animals and created an arteriovenous fistula. He also made observations on patients with AVM. He reported that the arterial pressure was low in the fistula, the venous pressure was high in the vicinity of the fistula, the distribution of the blood deteriorated and blood stealing phenomena were present. He also asked whether or not the controlateral cervical region was underfed and if autoregulation had deteriorated.

We consider a mathematical model of the circle of Willis (Fig. 2) comprising all segments of the circle, each segment being modelled mathematically by a system of three equations: the one-dimensional mass-conservation equation; the one-dimensional momentum-conservation equation;

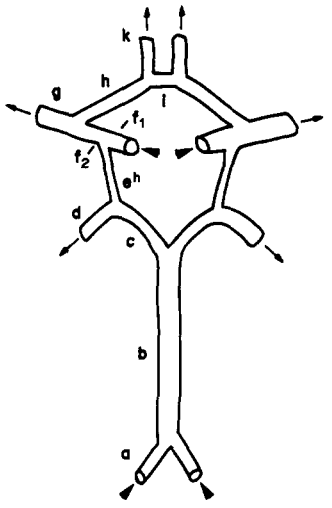

Fig. 1. Circle of Willis. a: vertebral arteries. b: (1): basilar. c: (2–18): posterior cerebral arteries (pre-communicating parts). d: (3–17): posterior cerebral arteries (post-communicating parts). e: (4–16): posterior communicating arteries. f_1: (5–15): internal carotid arteries (pre-communicating parts). f_2: (6–14): internal carotid arteries (post-communicating parts). g: (7–13): medial cerebral arteries. h: (8–12): anterior cerebral arteries (pre-communicating parts). i: 10: anterior communicating arteries. k: (9–11): anterior cerebral arteries (post-communicating parts).

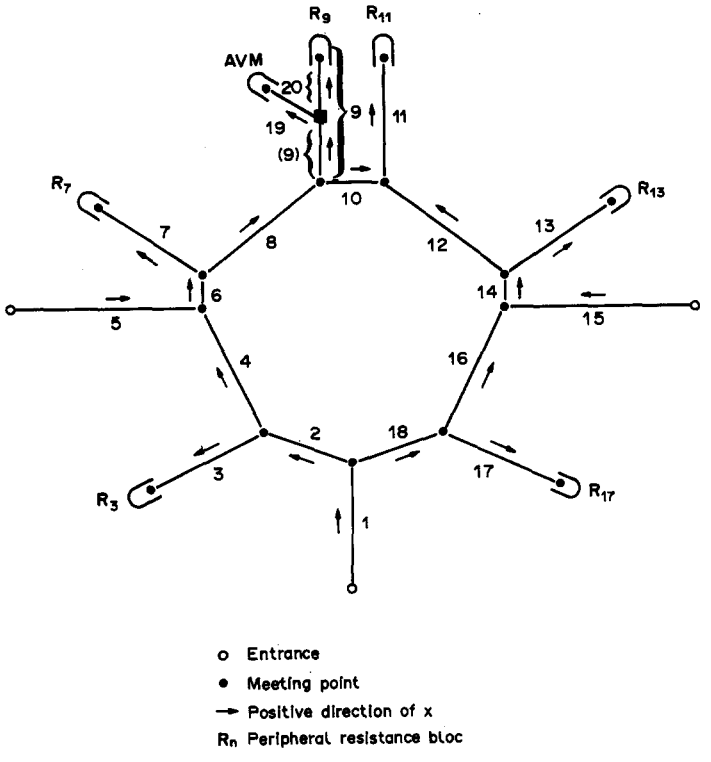

Fig. 2. Mathematical model of the circle of Willis.

and a functional relationship between pressure and the cross-section of the segment expressing the vessel's wall elasticity.

Each efferent vessel is terminated by a lumped (peripheral) resistance (R_i). We thus express the outflow in terms of the pressure difference between the vessel's extremity and the terminal bed or vein. The aortic segments were modelled as uniform, circular, distensible tubes. The blood is considered as an incompressible, viscous, Newtonian fluid. Table 1 lists the anatomical names and dimensions (in cm) in relation to the model. Note that the arrows indicate the positive direction of the flow.

We write for each segment the laws of mass and momentum for a one-dimensional flow:

$$\frac{\partial A}{\partial t}+\frac{\partial}{\partial x}(AU)=0 \tag{1}$$

$$\rho\left(\frac{\partial U}{\partial t}+U\frac{\partial U}{\partial x}\right)=-\frac{\partial P}{\partial x}+F;\quad F=-\frac{8\pi\mu U}{A}. \tag{2}$$

These equations involve three unknown functions, namely the velocity, U, the cross-sectional area of the segment, A, and the pressure P. The above functions depend on time (t) and on the axial coordinate (x).

The expression of the force F in equation (2) represents the effects of blood viscosity (μ stands for the dynamic viscosity coefficient and ρ for the density of blood). It is the Poiseuille formula for the resistance for laminar flow under steady-flow conditions in a circular tube. For small values (<10) of the dimensionless parameter $\alpha(\alpha = R\sqrt{\omega\rho/\mu}$, where R is the vessel's radius and ω is the angular frequency of the oscillatory motion), this formula can be used in pulsatory flow conditions [26, 27].

Table 1. Anatomical names and dimensions of the model segments

Arteries	Segment	Internal diameter (cm)	Length (cm)
Internal carotid	5–15	0.5	12
Internal carotid (second part)	6–14	0.5	0.5
Posterior communicating	4–16	0.1	1.5
Posterior cerebral (pre-communicating part)	2–18	0.2	1
Posterior cerebral (post-communicating part)	3–17	0.2	5
Anterior cerebral (pre-communicating part)	8–12	0.25	1.5
Anterior cerebral (post-communicating part)	9–11	0.25	5
Anterior communicating	10	0.1	0.4
Basilar	1	0.3	5
Medial cerebral	7–13	0.4	1.5
AVM (branch of the post-communicating part of the cerebral anterior artery)	19	0.25	2
Terminal part of the anterior cerebral	20	0.25	2
Anterior cerebral (post-communicating part)	9	0.25	3

The set of equations (1) and (2) was completed by a relation expressing the tube's cross-sectional area as a function of pressure. It is a relation of the vessel wall elasticity, chosen as follows:

$$A = A(P) = A_0\{1 + \beta(P - P_d)\}; \quad A_0 = A(P_d),$$

with the property $dA/dP > 0$; P_d is the diastolic pressure (80 mmHg) and β is an elasticity coefficient chosen equal to the value $1.887 \times 10^{-6}\,cm^2/dyn$, so that the cross sectional area is in agreement with experimental data [28–30].

3. NUMERICAL SOLUTION

The previous equations constitute a hyperbolic quasilinear system. In fact, we obtained as many sets of equations as segments included in our configuration. We then specified the proximal, distal and internal boundary conditions.

(i) We prescribed the variation of pressure at the entrances of our configuration as a function of time (pressure signal in the brachiocephalic artery, Fig. 3),

$$P(0, t) = F(t);$$

or as a constant,

$$P(0, t) = P_m(= \text{mean of } F(t) \text{ over a cardiac cycle}).$$

(ii) We imposed the continuity of pressure at the points where at least two segments meet. That means that pressures are equal in the proximity of the meeting point. For example, in the case of a bifurcation we write:

$$P_1(L_1, t) = P_2(0, t) = P_3(0, t),$$

where L_1 stand for the length of the segment arriving at the bifurcation and 0 for the entrances of the segments leaving the bifurcation.

(iii) We imposed mass continuity at the point where two or more segments meet, in the case of a bifurcation we write:

$$Q_1(L_1, t) = Q_2(0, t) + Q_3(0, t),$$

where Q stands for the instantaneous volume flux ($Q = AU$).

(iv) In the case of the distal boundaries (exits of our configuration or lumped resistance blocks), we took the pressure P_v at the venous end of the capillary

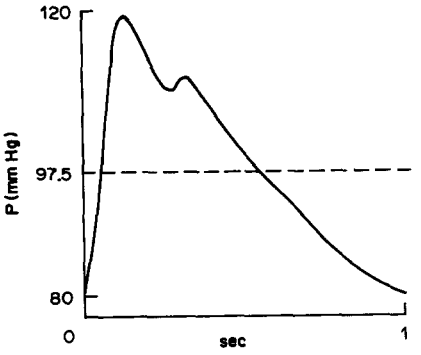

Fig. 3. Pressure signal.

as a constant equal to 10 mmHg, the pressure gradient $P(L,t) - P_v$, the peripheral resistance R_L and we express the whole as follows:

$$R_L = \frac{P(L,t) - P_v}{Q(L,t)},$$

where $Q(L,t) = A(L,t)U(L,t)$ is the volume flux at the end (L) of the segment arriving at the resistance block.

Once the physiological parameters were specified (heart rate 1 Hz, input signal of pressure $F(t)$, density of blood $\rho = 1\,\text{g/cm}^3$, dynamic viscosity $\mu = 0.03\,\text{dyn s cm}^{-2}$), we solved the system of equations by the Lax–Wendroff finite-difference scheme [31–33].

In order to adjust the values of the peripheral resistance blocks, we consider the total flow through the circle of Willis configuration equal to $12.5\,\text{cm}^3/\text{s}$, the mean of the total flux values available in the literature (10–15 cm^3/s). We then made the assumption that the flow in the efferent vessels is distributed in accordance with the weight of the brain tissue irrigated by each vessel. We choose the ratios 6 : 3 : 4 for the anterior, middle and posterior peripheral resistance block values, as has been done previously by a number of authors [10, 12, 16].

Under steady-flow conditions, imposing a constant pressure source equal to the mean value of the pressure signal, over a cardiac cycle, we adjusted the peripheral resistances (R). We found the values 78,000, 39,000 and 52,000 dyn s cm^{-5} for the anterior, middle and posterior resistance blocks, respectively, and a total flux of $12.8\,\text{cm}^3/\text{s}$ in the afferent vessels (the basilar artery and the two ICAs); (experiment N).

The numerical calculations were started with initial conditions of zero flow and constant pressure (venous pressure) throughout the configuration. We then drove the system to its final configuration by imposing a constant pressure source (97.5 mmHg) at the entrances (inlets) of our system.

We showed in the previous sections how we simulated the vasculature of the cerebral circulation in the circle of Willis and its vicinity, using a finite-difference numerical method. Preliminary results indicate the usefulness of the model in simulating the pressure and the flow distribution in the normal case (normal cerebral circulation, N). Figure 4 shows the division of the flow in the afferent and the efferent vessels, respectively, under steady-flow conditions in the normal case.

The results of the experiments show the role of the posterior communicating (Poc) artery. The magnitude of the flow ($-0.1722\,\text{cm}^3/\text{s}$) indicates that the Poc artery plays the role of an anastomosis, in the case of a redistribution of the flow in the circle as a result of the existence of a vascular lesion (Table 2, normal case). In the normal case, the flow in the Poc artery is towards the posterior cerebral artery, the direction depending largely on the value of the peripheral resistances in the vicinity. The symmetry of our model resulted in a zero flow in the anterior communicating artery CoA.

We simulated three types of AVMs:

(a) An AVM vascularized by the anterior cerebral artery (Ca).
(b) An AVM vascularized by the middle cerebral artery (Cm).
(c) An AVM vascularized by both the Ca and Cm arteries.

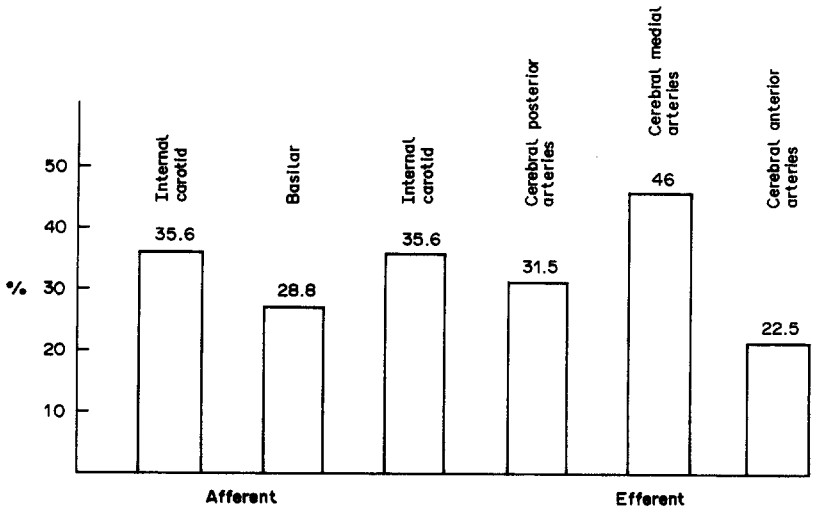

Fig. 4. Division of flow in the afferent and efferent vessels as a percentage of the total cerebral blood flow.

Experiments were carried out with a steady pressure source in order to evaluate the effect of the presence of the AVM on the flow distribution and the compensatory capacity of the circle of Willis.

Additional experiments, not reported here, showed that the volume flux in the AVM is a function of its volume or of the value of the resistance simulating the AVM. They showed also a strong correlation between the site of the AVM and its volume flux.

The general effects of the AVM are clear. We report in Table 2 the volume fluxes in the middle of the segments for an AVM (whose value was set equal to 5000 dyn s cm^{-5}) vascularized by a branch of the post-communicating part of the anterior cerebral artery (S1).

The decrease in the local resistance, as a consequence of the presence of the AVM, causes an increased flow in the internal homolateral carotid artery (CIh) and, to a lesser extent, in the internal controlateral carotid artery (CIc). Thus, the AVM is vascularized also, through the CoA.

The flow direction in the Poc arteries is towards the post-communicating part of the posterior cerebral arteries, but its flux has decreased significantly (98%).

Table 2. Volume fluxes (cm^3/s) in the middle of the segments

Experiment codes	Segments									Total cerebral flow
	1	2–18	3–17	4–16	5–15	6–14	7–13	8–13	9–11	(1 + 5 + 15)
N	3.709	1.854	2.027	−0.1722	4.581	4.408	2.9609	1.4479	1.447	12.871
S1	3.869	2.002	2.023	−0.0275	17.219	17.198	2.886	14.312	16.024	27.344
		1.867	2.025	−0.1579	6.256	6.098	2.951	3.146	1.434	
S2	4.734	2.893	1.999	0.893	11.866	12.759	2.431	10.328	13.639	24.446
		1.841	2.014	−0.173	7.846	7.673	2.942	4.731	1.419	
S3	3.867	2.021	2.023	−0.00196	18.679	18.677	2.877	15.8		27.133
		1.846	2.025	−0.178	4.587	4.409	2.961		1.448	
S4	4.889	3.095	1.995	1.1005	13.907	15.007	2.316	12.691		23.423
		1.794	2.012	−0.218	4.627	4.408	2.961		1.448	
S5	6.0797	4.348	1.961	2.387	6.232	8.619	1.345	7.275		16.9847
		1.732	1.997	−0.265	4.673	4.408	2.96		1.448	

Experiment codes	20(9)	19 (AVM)	10	Internal diameter of segment 5	
N	1.447	—	0	0.5	Normal case
S1	1.1025	14.922	−1.713	0.5	AVM
S2	0.937	12.7017	−3.311	0.3	AVM + reduction of diameter of segment 5
S3	1.087	14.713	—	0.5	AVM + obstruction of anterior communicating artery
S4	0.872	11.819	—	0.3	AVM + reduction + obstruction
S5	0.501	6.773	—	0.2	AVM + reduction + obstruction

Numerical experiments have been conducted to answer the following questions:

(a) The reduction of the cross-sectional area of the CIh is sufficient for reducing the volume flux in the AVM (experiment S2, the diameter of the CIh is taken as equal to 0.3 cm). This experiment corresponds to reducing the flow by means of a special clamp, described previously by Pertuiset *et al.* [22].
(b) The obstruction of the CoA reduces significantly the volume flux in the AVM (experiment S3); this experiment corresponds to placing an Aesculap clip on that vessel.
(c) The reduction of the cross-sectional area combined with an obstruction of the CoA, reduces significantly the volume flux in the AVM (experiments S4 and S5, the diameters of the CIh are taken equal to 0.3 and 0.2 cm, respectively).

These experiments will lead us to a clearer picture of the mechanisms underlying the presence of an AVM and suggest some therapeutic measures.

The general effects of the first experiment (reduction of the CIh's sectional area) was that the volume flux in the AVM is not diminished significantly as a result of the amount of blood arriving by the CIc through the CoA.

The results of the next experiment (S3), obstruction of the CoA, showed the increase in the volume flux in the CIh when the flow in the CoA is obstructed. The mechanism is clear. The increase is due to the fact that the CIh has to deliver blood for both the carotid arteries. The direction of flow in the homolateral Poc artery is reversed.

Obviously, experiments S2 and S3 show that it is not possible to reduce the volume flux in the AVM by obstructing the CoA or by reducing the CIh's sectional area. The association of the above two experiments (S4 and S5) diminishes the volume flux in the AVM by more than 50% (Table 2).

4. DISCUSSION AND CONCLUSION

The results of our experiments show the effect of the existence of an AVM and the effect of the two-stage operation.

The results of our experiments are qualitatively comparable with the data available in the literature [34]. We focused our attention mainly on the following questions:

1. What is the behaviour of our model under steady-flow conditions in the normal case?
2. How does the model react when an AVM is present?
3. What are the effects of the cross-sectional area of the CIh and the obstruction of the CoA on the volume flux in the AVM and on the model's behaviour?

The results of our experiments show that the flux in the efferent vessels of our model (basilar arteries and ICAs) is mainly influenced by the ratio of the peripheral resistances. The decreased resistance in the region of the AVM produces an increased flow in the homolateral segments.

In the vicinity of the AVM (terminal part of the post-communicating part of the anterior cerebral artery) we observed a blood stealing phenomenon (the volume flux decreased by 23.808%), as shown in Table 2 (segment No. 20). The volume flux in the AVM was reduced by more than 50% when we combined the reduction of the CIh's sectional area and the obstruction of the CoA. In this case the blood stealing increased up to 65.38%.

Naturally, our model does not include other important parameters of the cerebral circulation, such as the autoregulatory capability or the availability of collaterals. Nevertheless, we think that this blood stealing phenomena must be taken into account by the surgeon performing the operation, as we described in the previous sections.

The situation becomes more complex as the number of the model parameters increases. So, the next step will be to include in our configuration and to use in the simulation, data of the cerebral circulation obtained by Doppler, radiography, CT or NMR methods.

REFERENCES

1. L. Rogers, The function of circulus arteriosus of Willis. *Brain* **70,** 171–178 (1947).
2. N. Avmon and E. A. Bering, A plastic model for the study of pressure changes in the circle of Willis and major cerebral arteries following arterial occlusion. *J. Neurosurg.* **18,** 361–365 (1961).
3. V. L. Streeter, W. F. Keitzer and D. F. Bohr, Pulsatile pressure and flow through distenssible vessels. *Circulation Res.* **XIII,** 3–21 (1963).
4. K. D. Murray, Dimensions of the circle of Willis and dynamic studies using electrical analogy. *J. Neurosurg.* **21,** 26–34 (1964).
5. V. A. Fasano, A. Portulupi and B. Broggi, Study of cerebral hemodynamics by analogic models. *Vasc. Dis.* **3,** 89–99 (1966).
6. M. E. Clark, J. D. Martin, R. A. Wenglers, W. A. Himwich and F. M. Knapp, Engineering analysis of the hemodynamics of the circle of Willis. *Archs Neurol.* **13,** 173–182 (1965).
7. M. E. Clark, W. A. Himwich and J. D. Martin, Simulation studies of factors influencing the cerebral circulation. *Acta neurol. scand.* **43,** 189–204 (1967).
8. M. E. Clark, W. A. Himwich and J. D. Martin, A comparative examination of cerebral circulation models. *J. Neurosurg.* **29,** 484–494 (1968).
9. M. E. Clark and R. H. Kufahl, Simulation of cerebral macrocirculation. In *Cardiovascular System Dynamics*, pp. 380–390. MIT Press, Cambridge, Mass. (1978).
10. W. A. Himwich, G. Galesburg, R. A. Wenglarz, J. D. Martin and M. E. Clark, The circle of Willis as simulated by an engineering model. *Archs Neurol.* **13,** 164–172 (1965).
11. W. A. Himwich and M. E. Clark, Simulation of the flow and pressure distribution in the circle of Willis. In *Pathology of Cerebral Microcirculation* (Ed. J. Cervos-Navarro), pp. 140–152, de Gruyter, New York (1974).
12. J. C. Chao and N. H. C. Hwang, A dynamic model of the circle of Willis. *J. Biomech.* **4,** 141–147 (1971).
13. J. C. Chao and N. H. C. Hwang, Functional dynamics of the circle of Willis. *J. Life Sci.* **2,** 81–88 (1972).
14. J. Duros and P. Nadvornik, Investigation of cerebral blood circulation on computer model. *J. neurosurg. Sci.* **21,** 243–246 (1977).
15. B. Hillen, T. Baasbeek and H. W. Hoogstraten, A mathematical model of the flow in the posterior communicating arteries. *J. Biomech.* **15,** 441–448 (1982).
16. B. Hillen, H. W. Hoogstraten and L. Post, A mathematical model of the flow in the circle of Willis. *J. Biomech.* **19,** 187–194 (1986).
17. R. H. Kufahl and M. E. Clark, A circle of Willis simulation using distensible vessels and pulsatile flow. *Trans. ASME J biomech. Engng* **107,** 112–122 (1985).
18. R. Collins and J. A. Maccario, Blood flow in the lung. *J. Biomech.* **12,** 373–395 (1979).
19. R. Collins and M. Zagzoule, Blood flow in the human brain. In *Biofluid Mechanics*, Vol. 2. Plenum Press, New York (1982).
20. M. Zagzoule and J. Marc-Vergnes, A global mathematical model for the cerebral circulation in man. *J. Biomech.* **9,** 1015.
21. D. Ancri and B. Pertuiset, Mesure des vitesses sanguines instantanées dans les artères carotides internes par Doppler pulsé dans les malformations artérioveineuses cérébrales. *Neurochirurgie* **31,** 1–6 (1985).
22. B. Pertuiset, D. Ancri *et al.*, Radical surgery in cerebral AVM tactical procedures based upon hemodynamic factors. In *Advances in Technical Standards in Neurosurgery*, Vol. 10. Springer, New York (1983).
23. B. Pertuiset, D. Ancri *et al.*, Conséquences hémodynamiques du shunt vasculaire dans les malformations artério-veineuses intra-cérébrales sus-tentorielles. *J. Neuroradiol.* **12,** 165–178 (1985).
24. J. M. Nies, The haemodynamic effect of an intracranial arteriovenous anomaly, a Dopper haematochographic study. *Clin. Neurol. Neurosurg.* **79,** 29–45 (1979).
25. W. Hassler, Hemodynamic aspects of cerebral angiomas. *Acta Neurochir. Suppl.* **37.**
26. J. R. Womersley, Cited in Ref. [27].
27. D. A. McDonald, *Blood Flow in Arteries.* Arnold, London (1974).
28. K. Hayashi, H. Handa, S. Nagasawa, A. Okumura and K. Moritake, Stiffness and elastic behavior of human intracranial and extracranial arteries. *J. Biomech.* **13,** 175–184 (1980).
29. D. E. Busby and A. C. Burton, The effect of age on the elasticity of the major brain arteries. *Can. J. Physiol. Pharmac.* **43,** 185–202 (1965).
30. B. M. Learoyd and M. G. Taylor, Alterations with age in the viscoelastic properties of human arterial walls. *Circulation Res.* **18,** 278–292 (1966).
31. C. M. Dafermos, Hyperbolic systems of conversation laws. In *Systems of Nonlinear Partial Differential Equations* (Ed. J. M. Ball), pp. 25–70. Reidel, New York (1983).
32. R. J. Diperna, Finite difference schemes for conservation laws. *Communs pure appl. Math.* **XXV,** 379–450 (1982).
33. R. Richtmyer and K. W. Morton, *Difference Methods for Initial-value Problems*, 2nd edn. Interscience, New York (1967).
34. C. Papapanayotou, Modélisation mathématique de la circulation sanguine cérébrale et application aux malformations artérioveineuses (MAV). Thèse de Doctorat de l'Université Paris 6, Paris (1988).